UC Irvine
UC Irvine Previously Published Works

Title

Parametric Thermodynamic Analysis of a Solid Oxide Fuel Cell Gas Turbine System Design Space

Permalink

https://escholarship.org/uc/item/3s01x4p6

Journal

Journal of Engineering for Gas Turbines and Power, 132(7)

ISSN

0742-4795

Authors

Tarroja, Brian
Mueller, Fabian
Maclay, Jim
et al.

Publication Date

2010-07-01

DOI

10.1115/1.4000263

Copyright Information

Peer reviewed

Parametric Thermodynamic Analysis of a Solid Oxide Fuel Cell Gas Turbine System Design Space

Brian Tarroja

Fabian Mueller[1]
e-mail: fm@nfcrc.uci.edu

Jim Maclay

Jacob Brouwer

National Fuel Cell Research Center,
University of California,
Irvine, CA 92697-3550

A parametric study of a solid oxide fuel cell-gas turbine (SOFC-GT) hybrid system design is conducted with the intention of determining the thermodynamically based design space constrained by modern material and operating limits. The analysis is performed using a thermodynamic model of a generalized SOFC-GT system where the sizing of all components, except the fuel cell, is allowed to vary. Effects of parameters such as pressure ratio, fuel utilization, oxygen utilization, and current density are examined. Operational limits are discussed in terms of maximum combustor exit temperature, maximum heat exchanger effectiveness, limiting current density, maximum hydrogen utilization, and fuel cell temperature rise. It was found that the maximum hydrogen utilization and combustor exit temperature were the most significant constraints on the system design space. The design space includes the use of cathode flow recycling and air preheating via a recuperator (heat exchanger). The effect on system efficiency of exhaust gas recirculation using an ejector versus using a blower is discussed, while both are compared with the base case of using a heat exchanger only. It was found that use of an ejector for exhaust gas recirculation caused the highest efficiency loss, and the base case was found to exhibit the highest overall system efficiency. The use of a cathode recycle blower allowed the largest downsizing of the heat exchanger, although avoiding cathode recycling altogether achieved the highest efficiency. Efficiencies in the range of 50–75% were found for variations in pressure ratio, fuel utilization, oxygen utilization, and current density. The best performing systems that fell within all design constraints were those that used a heat exchanger only to preheat air, moderate pressure ratios, low oxygen utilizations, and high fuel utilizations. [DOI: 10.1115/1.4000263]

1 Introduction

Due to high efficiency and low emissions performance characteristics, solid oxide fuel cells (SOFC) are emerging as an alternative platform for electric power generation. Hybrid SOFC gas turbine technology is remarkably attractive, achieving fuel-to-electricity conversion efficiencies greater than either an individual SOFC or gas turbine cycle. The current analyses focus on the overall design space and performance of hybrid systems as fueled by pure hydrogen. Hydrogen is used as the fuel in these analyses for three reasons: (1) current integrated coal gasification fuel cell systems that include CO_2 sequestration may provide a relatively pure hydrogen stream to the fuel cell power block, (2) aerospace applications consider the use of hydrogen fuel, and (3) use of hydrogen fuel reduces the number of variables in the design space sufficient for thorough analysis in a single paper. Other fuels and fuel processing may be considered in future analyses. Thermodynamic analysis capabilities were developed, as a result, to analyze the design space of two particular hydrogen-fueled hybrid applications:

(1) Stationary power applications where the fuel (natural gas, oil, or coal) is converted to hydrogen prior to electrochemistry and/or combustion to effectively capture gaseous carbon emissions. Such ideas are seriously being considered in by U.S. Department of Energy programs, to sequester carbon emissions from large centralized coal power plants [1,2].

(2) Auxiliary or propulsion power units for long endurance aerospace applications such as unmanned aerial vehicles. In aerospace applications, on board fuel preprocessing is heavy, which often is the limiting factor for implementing SOFC-GT systems [3,4]. On the other hand, the high efficiency of SOFC-GT hybrid systems reduces the amount of fuel that must be carried on board, making hydrogen hybrid systems attractive due to the excellent gravimetric energy density of hydrogen [5–7].

In both of these applications, the SOFC, gas turbine, and other components will have to be effectively integrated and controlled within a certain design space. Before this can be achieved, it is necessary to understand the fundamentals of: (1) optimal thermodynamic design characteristics, (2) material and operating limitations that are inevitably imposed on hybrid systems, and (3) system design tradeoffs. Once the challenges are understood fundamentally the design space can be identified, which makes it possible to better evaluate how and if existing gas turbine technologies can be used effectively in SOFC/GT hybrid systems and whether new or modified gas turbine designs are required.

It is important to understand that this study explores the design space of hybrid systems rather than the operating space. The size of subcomponents, such as the compressor, turbine, and heat exchangers, are allowed to vary throughout the analyses. Before a particular system is analyzed, the design of the nominal operating point, system configuration, operating pressure, hydrogen utilization, oxygen utilization, and gas preheating effects on the system efficiency as well as system design operating point limitations

must be understood. An important and new contribution of the current analyses is the imposition of a full suite of reasonable constraints on the design space.

2 Background

Previous SOFC/GT hybrid systems thermodynamic analyses have focused upon developing insights into:

(1) Effects of various system configurations [2,8,9].
(2) Effects of operating conditions [2,8,10,11].
(3) Trade-offs between efficiency and cost [9,10].

Calise et al. and Chan et al. [10–12] performed exergy-based analyses of hybrid systems to single out system components that exhibit the greatest degree of irreversibility, determining that the SOFC stack was the largest contributor. Various system configurations were considered, such as internal versus external reforming schemes [13] with anode gas recirculation to provide the reforming steam. Optimization of particular configurations was investigated as well as different schemes for meeting the desired operating parameters, such as cathode and turbine inlet temperatures.

Rao and Samuelsen [9] performed a detailed thermodynamic analysis of a tubular solid oxide fuel cell hybrid system for coal based application focusing on optimal system configurations on the bases of efficiency and cost.

Zhang et al. [8,14] discussed the different schemes of recuperation and heat recovery, comparing the effects of blower-based recirculation versus the use of a heat exchanger for preheating the cathode inlet air. This group discovered that, with their assumptions of negligible system pressure drops and the use of an existing gas turbine design, the use of booster-based recirculation yielded higher system efficiencies overall when compared with the use of a heat exchanger. However, they noted that the improvement of the gas turbine components would make the efficiency of the heat exchanger based system higher than that of the cathode recirculation booster-based system.

Kuchonthara et al. [15] discussed other recuperation schemes, such as steam recuperation, and compared overall performance to the case with heat recuperation alone.

Parametric analyses have been conducted with the consideration of fuel cell operating temperature, turbine inlet temperature [13], and operating pressure [16] to study the effects of these parameters on system performance. General design studies have also been conducted taking into account system compatibility issues [17,18], and different methods of optimization [19,20].

Park et al. [17,21] compared the performance of ambient pressure systems versus pressurized systems, discovering that pressurized systems have a distinct efficiency advantage over ambient pressure systems due to increased cell voltage and better utilization of the gas turbine component of the system.

Transient models for controls and dynamic modeling of SOFC-GT systems have also been developed to simulate real time operation [22–25]. Compatibility and coupling issues between current SOFC and GT subsystems are currently being investigated [17,26]. Performance analyses have demonstrated theoretical fuel-to-electricity conversion efficiencies in the range of 70–80% (net ac) [27,28], with projected overall efficiencies over 80% with the use of waste heat recovery [29].

While the above literature review demonstrates that SOFC-GT hybrid systems have been extensively studied in the past, no previous study has generally investigated the thermodynamics of the complete design space with a full suite of concomitant realistic operating constraints. Generally, previous research has focused on either a particular system, or a particular operating condition or specific off-design conditions. While the design space issues investigated in this paper have been considered in various forms in various studies, they have not all been considered on the same basis and with realistic operating constraints for the purpose of mapping a general hybrid system design space. By considering the
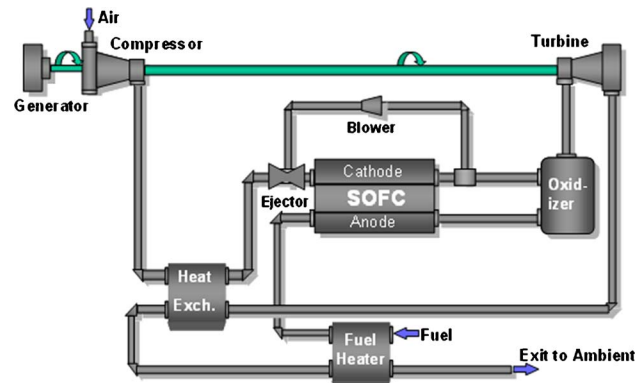

Fig. 1 Pure hydrogen SOFC/GT hybrid system diagram

design issues simultaneously and on the same basis (e.g., environmental conditions, scale, fuel cell size, compressor and turbine design, compressor and turbine efficiency), valuable insights can be made regarding design space tradeoffs and optimal design considerations. The effect of multiple parameters, such as fuel utilization, oxygen utilization, current density, pressure ratio, and different schemes of recirculation are studied within the constraints to determine their realizable effects on the optimal operating design point.

3 System Configuration and Modeling

3.1 Modeling Methodology. The developed model is based on conservation of mass, species, energy and momentum along with heat transfer, chemical kinetics, and electrochemistry. Conservation and transport equations are developed for each system component as described in the remainder of this section. The set of equations and input variables are solved using the ENGINEERING EQUATION SOLVER (EES) package. The basic function provided by EES is the solution of a set of coupled algebraic equations. A major difference between EES and existing equation solving programs is that EES provides many built-in mathematical and thermophysical property functions. For example, the steam tables are implemented such that any thermodynamic property can be obtained from a built-in function call in terms of any two other properties. Air tables are built-in, as are psychrometric functions and thermodynamic data for many common gases. EES was particularly attractive for this work due to the program's capability for performing parametric studies. Selected variables can be parametrized in spreadsheet-like tables, which EES solves using the programmed model.

Specifically EES uses a variation in Newton's method to solve systems of nonlinear algebraic equations [30]. Specific details regarding the algorithm can be found in the EES manual. System simulation solutions were obtained by solving a total of 211 equations simultaneously in EES. EES allows equations to be entered in any order with unknown variables placed anywhere in the equations; EES automatically reorders the equations for efficient solution. All of the model governing equations solved using EES are presented in this document.

3.2 System Configuration. A hydrogen-fueled topping solid oxide fuel cell gas turbine hybrid system shown in Fig. 1 was considered for the current analyses, which is a typical configuration for SOFC/GT hybrid systems. Air from the compressor is preheated by the exhaust air as well as recirculated cathode off-gas (by an ejector or blower) before entering the fuel cell. The amount of air recirculated by the ejector and blower can be varied as a design parameter.

Hydrogen is preheated before entering the stack module in a fuel recuperator by heat exchange with the system exhaust. Anode off-gas is oxidized by reaction with cathode off-gas in the com-

Table 1 Important model parameters

Fixed input parameters	Value
Number of fuel cell stacks (input)	150
Fuel cell area	400 cm^2
Cathode inlet temperature	1000 K
Exchange current density	300 mA/cm^2
Compressor stage polytropic efficiency	0.70
Turbine stage isentropic efficiency	0.70
Blower isentropic efficiency	0.80

Variable input parameters	Range
Compressor pressure ratio	2–12
Current density	0–1450 mA/cm^2
Oxygen utilization	0.1–0.3
Ratio of recirculation	0–1
Fuel utilization	0.65–0.90

bustor, directly downstream of the fuel cell, with combustor exhaust entering the turbine. Important model parameters are presented in Table 1. The total system power range varies depending upon the parameter inputs selected. This study targets systems in the 50 MW range. The GT-SOFC hybrid model was constructed using EES [31], making use of its parametric table, thermodynamic property and analysis capabilities to perform the calculations.

3.3 Parametric Analysis. As shown in Fig. 1, the model contains 12 state points. The model is comprised of 211 equations and 211 variables, five of which are variable input parameters. The system of equations is solved simultaneously using EES. The model input parameters are listed in Table 2. In all cases considered the fuel cell size and fuel cell anode and cathode inlet temperature were held constant. The fuel cell current, hydrogen and oxygen utilization, as well as the system pressure ratio and recirculation were each varied parametrically.

From these inputs, the fuel cell, combustor, gas turbine, and recuperator exhaust mole fractions and temperatures as well as the power generated from the fuel cell and gas turbine were determined, mapping the design space of the hybrid system. The fuel cell current has direct effects on the fuel and oxygen consumption, as well as the amount of heat generated. The fuel and air flow rates of the system must be designed such that the fuel cell temperature is maintained, and a sufficient level of fuel and air are always present within the fuel cell. Therefore, fuel and oxygen flow rates are nondimensionalized to fuel and oxidant utilizations in this paper in order to decouple the effects of fuel and air flow rates on current. At the maximum power point, the fuel cell generates about 44 MW with the gas turbine power output at 23 MW for a power generating ratio of about 2:1.

The model easily allows changes and parametrization of any variable in the model. In the current analyses, fuel cell inlet temperatures are held constant because the design fuel cell operating temperature is typically fixed early in the design of a fuel cell system. The fuel cell operating temperature is dictated by the materials set and cell design, which fixes the durability and conduction properties of the fuel cell trilayer.

Table 2 Operating limits

Limiting factor	Operating constraint
Fuel cell cathode temperature rise	<200 K
Insufficient gas preheating	Heat Ex. Effectiveness <0.90
Combustor temperature	<1573 K
Fuel utilization	<90%

3.3.1 Model Assumptions. The following assumptions are made in the model development:

(1) Each of the system components are characterized by a single lumped temperature, pressure, and species mole fractions condition.
(2) Gas mixtures are comprised only of H_2, H_2O, N_2, and O_2.
(3) Each cell within a stack is assumed to operate identically, so that a single SOFC cell simulation is taken as representative and used to calculate full stack performance [32,33]. Fuel cell stacks are then added to scale-up in total FC system power capability.
(4) Activation polarization in the anode is neglected. Activation polarization in the cathode is at least an order of magnitude higher than that of the anode [34]. A single activation polarization equation is used to capture the effects of all physical and chemical processes that polarize the charge transfer process.
(5) In the fuel cell, all reactants generate their ideal number of electrons, and no fuel or oxidant crosses the electrolyte.
(6) Pressure drops in the fuel cell are calculated for laminar flow conditions.
(7) Hydrogen is provided at the required system pressure.
(8) Heat loss to the environment occurs only in the fuel cell and combustor components of the system.
(9) 100% fuel oxidation is assumed in the combustor.
(10) The system and component performance are calculated only for steady state conditions.
(11) All gases behave as ideal gases.
(12) Pressure drops in heat exchangers are considered negligible compared with the pressure drop in the fuel cell [35]

3.3.2 Conservation Equations

3.3.2.1 Energy. The energy balance for each component is calculated from the first law of thermodynamics as follows:

$$\sum \dot{m}_e h_e - \sum \dot{m}_i h_i = \dot{Q} - \dot{W} \tag{1}$$

From this equation the component exit enthalpy can be determined from inlet conditions, and the mass flow rate as determined from mass conservation.

Enthalpy is evaluated as sensible enthalpy plus enthalpy of formation accounting for any reaction energy associated with chemical and electrochemical reactions. The enthalpy of every state point is evaluated from temperature using built-in EES thermodynamic property functions. Work extracted from the system is taken as positive and heat into the system is taken as positive as shown in Eq. (1).

3.3.2.2 Species. Species conservation is applied in each component:

$$\sum \dot{N}_i x_i = \sum \dot{N}_e x_e + \dot{\vec{R}} \tag{2}$$

where $\dot{\vec{R}}$ is the molar reaction rate of each species in the system component of interest.

From the species conservation equation (2) applied to each component, exit mole fractions can be determined from the reaction rate, inlet conditions, and molar flow rate as determined from mass conservation.

3.3.3 Component Descriptions

3.3.3.1 Compressor. The design compressor air flow is determined from the fuel cell current and desired oxygen utilization as follows:

$$\dot{N}_{\text{air}} = \frac{1}{U_{O_2}} \cdot \frac{i}{1000} \cdot \frac{n\text{stacks}}{n \cdot F \cdot 0.21} \tag{3}$$

where $n$stacks represents the number of fuel cell stacks and U_{O_2} represents the oxygen utilization, taken to be an input parameter. Setting the oxygen utilization determines the system air flow rate for a given power condition. No reaction is assumed to take place in the compressor, hence the compressor exit mole fractions are the same as those at the inlet. The compressor exit temperature is determined from the compressor isentropic efficiency. The compressor isentropic efficiency is determined from the polytropic efficiency as presented in [36]:

$$\eta_c = \frac{\left(\dfrac{P_{\text{out}}}{P_{\text{in}}}\right)^{k-1/k} - 1}{\left(\dfrac{P_{\text{out}}}{P_{\text{in}}}\right)^{k-1/k-\eta_{\text{cp}}} - 1} \qquad (4)$$

where k is the specific heat ratio for air, $(P_{\text{out}}/P_{\text{in}})$ is the compressor pressure ratio, and η_{cp} is the polytropic efficiency of the compressor. Resolving the compressor isentropic efficiency in this fashion captures compressor pressure ratio affects on the isentropic efficiency. Compressors with higher pressure ratio will inherently have a lower isentropic efficiency. Polytropic efficiency captures the general trend of decreased compressor efficiency with increased pressure ratios and compression stages.

3.3.3.2 Ejector. An ejector is used to recirculate cathode off-gas to the fuel cell air inlet to increase the cathode inlet flow temperature. The cathode off-gas can be recirculated by use of an ejector (Venturi) to create suction at the expense of a pressure drop through the ejector. The ratio of recirculated flow to compressor flow (w as defined by Eq. (5)) can be varied by varying the ejector design resulting in various curves of pressure drop versus recirculated mass [37–40]. The recirculation ratio is defined as

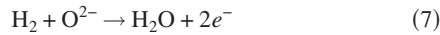$$w = \frac{m_{\text{recirc}}}{m_{\text{comp}}} \qquad (5)$$

where m_{recirc} is the mass flow rate of recirculated air and m_{comp} is the mass flow rate of air through compressor.

From momentum conservation, the ejector pressure drop must increase with increased recirculation ratio. In the model, the ejector pressure drop associated with air recirculation, is captured as follows:

$$\frac{P_3 - P_4}{P_4} = 0.25 \cdot w \qquad (6)$$

This is consistent with experimental results of ejector performance in SOFC systems as presented in [39,40] and is a good first approximation of ejector performance in SOFC systems in general.

3.3.3.3 Fuel cell. Standard pure hydrogen electrochemical reactions are captured in the fuel cell. The anode half reaction is

$$\text{H}_2 + \text{O}^{2-} \rightarrow \text{H}_2\text{O} + 2e^- \qquad (7)$$

and the respective cathode half reaction is

$$\tfrac{1}{2}\text{O}_2 + 2e^- \rightarrow \text{O}^{2-} \qquad (8)$$

The species reaction rates in the fuel cell are determined from Faraday's law as follows:

$$\dot{R}_{\text{O}_2} = -\frac{i}{1000} \cdot \frac{n\text{cells}}{n \cdot F} \qquad (9)$$

$$\dot{R}_{\text{H}_2} = -\frac{i}{1000} \cdot \frac{n\text{cells}}{n \cdot F} \qquad (10)$$

$$\dot{R}_{\text{H}_2\text{O}} = \frac{i}{1000} \cdot \frac{n\text{cells}}{n \cdot F} \qquad (11)$$

The species reaction rates in the fuel cell are proportional to the electrical current since the charge transfer must balance in the electrochemical reactions. This is convenient for resolving the fuel cell exit mole fractions because the fuel cell electrical current is a system input parameter. The stack inlet hydrogen flow rate is determined from the desired fuel cell current and hydrogen utilization using current-based-fuel-control as presented in previous work by Mueller et al. [25]:

$$\dot{N}_{\text{H}_2} = \frac{1}{U_f} \cdot \frac{i}{1000} \cdot \frac{n\text{cells}}{n \cdot F} \qquad (12)$$

The total hydrogen inlet molar flow to the system is then determined by multiplying the stack flow rate by the number of stacks.

From the fuel cell operating temperatures, exit species mole fractions, and fuel cell current, the fuel cell voltage can be determined by solving for the Nernst voltage and the corresponding activation, ohmic, and concentration voltage losses as follows:

$$V = V_{\text{Nernst}} - V_{\text{act}} - V_{\text{ohm}} - V_{\text{conc}} \qquad (13)$$

The Nernst voltage is evaluated as follows:

$$V_{\text{Nernst}} = -\frac{\delta G(T_{\text{fc}})}{n \cdot F} + \frac{R \cdot T_{\text{fc}}}{n \cdot F} \cdot \ln \frac{P_{\text{H}_2} \cdot P_{\text{O}_2}^{1/2}}{P_{\text{H}_2\text{O}}} \qquad (14)$$

With the fuel cell operating temperature (T_{fc}) evaluated as the average of the cathode inlet and outlet stream temperatures. The activation overpotential is determined from the Butler–Volmer equation with a charge transfer coefficient of 0.5, in the convenient form:

$$V_{\text{act}} = \frac{RT_{\text{fc}}}{F} \cdot \sinh^{-1}\left[\frac{j}{2 \cdot j_o}\right] \qquad (15)$$

Where j is the operating current density of the fuel cell and j_o is the exchange current density.

The concentration overpotential is evaluated as follows:

$$V_{\text{conc}} = -\frac{RT_{\text{fc}}}{n \cdot F} \cdot \ln\left[1 - \frac{j}{j_{\text{L}}}\right] \qquad (16)$$

where the limiting current density (j_{L}) is evaluated as in [41] as a function of pressure:

$$j_{\text{L}} = j_{\text{L}(1\ \text{atm})} \cdot \left(\frac{P_4}{P_{\text{atm}}}\right)^{0.35} \qquad (17)$$

The overall ohmic resistance losses are defined by the area specific resistance as a function of temperature based on the work presented by Kim [42]:

$$R_{\text{eff}} = 2 \cdot T_{\text{fc}} \cdot \exp\left(7509.6 \cdot \frac{1}{T_{\text{fc}}} - 25.855\right) \qquad (18)$$

The current SOFC cell model used was not directly validated against measured performance characteristics, however, the equations that define the model are taken from previous models that have been validated by comparison to measurements [41,42].

The overall fuel cell energy balance is as follows:

$$\dot{m}_{\text{H}_2}h_{\text{H}_2} + \dot{m}_{\text{air}}h_{\text{air}} = \dot{m}_{\text{cathode,out}}h_{\text{cathode,out}} + \dot{m}_{\text{anode,out}}h_{\text{anode,out}} + \dot{W}_{\text{FC}}$$
$$+ \dot{Q}_{\text{loss}} \qquad (19)$$

$$\dot{W}_{\text{FC}} = V \cdot I \cdot n\text{cells} \qquad (20)$$

The cathode and anode exit temperature are assumed to be equal. Enthalpies are evaluated based on temperature utilizing built-in EES thermal functions using National Institute of Standards and Technology-Joint Army, Navy, Air Force (NIST-JANAF) thermodynamic property data for many common gases. Note that the fuel cell operating temperature is assumed to be the average of the cathode inlet and outlet temperatures. Heat losses were modeled in the fuel cell based on and effective overall thermal conductance

(U) and the temperature difference between the fuel cell (or combustor) and ambient conditions as follows:

$$\dot{Q}_{\text{lost}} = U_{\text{ht}} \cdot (T_{\text{fc}} - T_{\text{amb}}) \qquad (21)$$

Note that this form of equation captures the effects of component temperature changes without resolving the physics of overall conduction, convection, and natural convection heat transfer processes. Rather, in a manner similar to a heat transfer resistance network simplification, overall heat transfer is captured by one coefficient. According to Balan et al. [35], the fuel cell and combustor together should exhibit approximately 6.3% total heat loss with respect to the lower heating value of the fuel into the fuel cell. An overall thermal conductance coefficient of 0.010 kW/K in the fuel cell and 0.0038 kW/K in the combustor was found to result in approximately 6.3% total heat loss at typical operating conditions. These overall conductance values were used throughout the study.

The pressure drop within the fuel cell was evaluated from the Darcy friction factor for laminar fully developed flow in a pipe (i.e., 64/Re) at constant pressure and temperature. The friction factor was adjusted to produce a 3% pressure drop through the fuel cell at maximum system flow conditions. A 3% pressure drop is consistent with results reported by Balan et al. [35]. Note that each fuel cell stack is arranged in a one-pass parallel flow configuration.

3.3.3.4 Turbine. The turbine exit temperature is determined from the turbine inlet temperature, pressure ratio, and turbine isentropic efficiency. The turbine isentropic efficiency is evaluated as in Ref. [36], resolving the effects of the number of stages, and pressure ratio on the turbine isentropic efficiency.

$$\eta_T = \frac{1 - \left[1 - \eta_{Ts} \cdot \left(1 - \left[\dfrac{P_{\text{out}}}{P_{\text{in}}} \right]^{k-1/k \cdot N_s} \right) \right]^{N_s}}{1 - \left[\dfrac{P_{\text{out}}}{P_{\text{in}}} \right]^{k-1/k}} \qquad (22)$$

where k is the specific heat ratio of air, N_s is number of turbine stages, and η_{Ts} representing the isentropic efficiency of each stage. A maximum pressure ratio per stage is set at 2.5.

3.3.3.5 Blower. The blower power is determined from its isentropic efficiency and the fuel cell pressure drop:

$$W_{\text{blower}} = - \frac{\dot{N}_{\text{blower}}}{\eta_{\text{blower}}} \cdot \frac{k \cdot R \cdot T}{k-1} \cdot \left[\left(\frac{P_{\text{out}}}{P_{\text{in}}} \right)^{k-1/k} - 1 \right] \qquad (23)$$

where T is the cathode exit temperature and η_{blower} is the isentropic efficiency of the blower. The blower exit temperature is further evaluated from the isentropic efficiency.

3.4 Operating Constraints. The operating constraints that were considered in order to determine the design space of the generalized system are presented in Table 2.

The combustor temperature is limited to less than 1573 K, which is the maximum temperature that modern turbine blade material sets that utilize thermal barrier coatings and internal cooling [43] can withstand in continuous operation. Note that turbine blade transpiration cooling is not considered. The fuel utilization in the fuel cell must remain below 90% to avoid risk of fuel depletion in the fuel cell [24,44,45]. At very high fuel utilizations, the Ni-YSZ anode material may begin to oxidize and change volume, introducing stresses in the trilayer which may break the fuel cell.

The heat exchanger effectiveness must remain below 90% to obey the second law of thermodynamics and to avoid the need for excessively large heat exchangers. The fuel cell cathode temperature rise (i.e., the temperature difference in the fuel cell cathode from the inlet of the stack to the exit of the stack) must remain below 200 K in order to minimize thermal stresses within the fuel cell. Since SOFC trilayer materials are ceramics, the fuel cell is
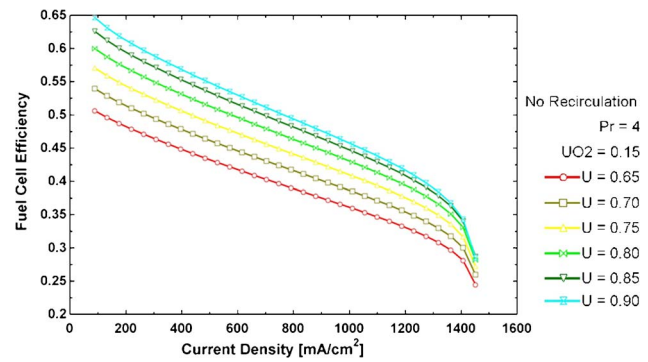

Fig. 2 Fuel cell efficiency versus current density for various fuel utilization conditions, no cathode gas recirculation, constant pressure ratio of 4 and oxygen utilization of 15%

not capable of withstanding the thermal stresses associated with large temperature gradients. The model presented in this paper does not resolve the cell temperature profile, but rather, uses the overall temperature difference as representative of the cell temperature gradient.

A design point is shaded out on the figures if the steady state operation at that design point requires operating parameters, which do not meet those constraints.

4 Results and Discussion

4.1 Design Space

4.1.1 Current and Utilization Variation. The fuel cell efficiency decreases monotonically with increasing current density in a manner reflecting the fuel cell polarization curve, as expected. Figure 2 presents the cell efficiency versus current density for various fuel utilization conditions, no cathode off-gas recirculation, a constant pressure ratio of 4, and oxygen utilization of 15%.

For the range of hydrogen utilizations considered, the fuel cell efficiency increases with increasing utilization. Although fuel cell efficiency continuously increases with increasing hydrogen utilization utilizations of 90% and above are not practically achievable, due to imperfect fuel distribution and the need for a margin of safety [46,47]. For these reasons the fuel utilization selected for best performance in this paper is 85%.

Figure 3 presents the system efficiency versus current density for various fuel utilization conditions showing applicable constraints as shaded areas. Note that the system efficiencies are highly influenced by the fuel cell efficiency as indicated by the dependence on fuel cell current density, which is representative of polarization curves. The system efficiency was found to increase
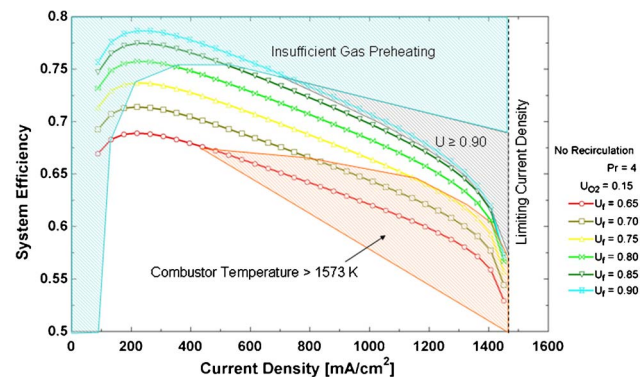

Fig. 3 System efficiency versus current density for various fuel utilization conditions showing applicable constraints (shaded areas)
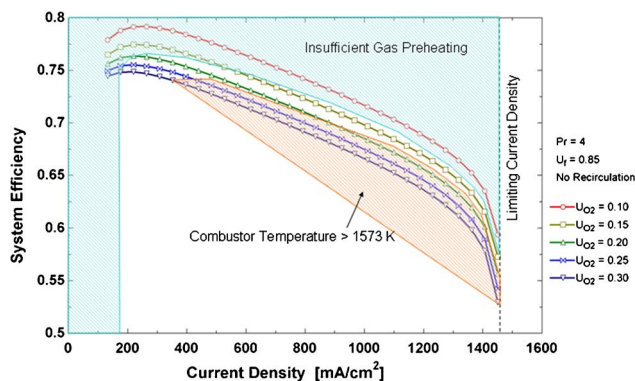
Fig. 4 System efficiency versus current density for various oxygen utilization conditions, constant pressure ratio of 4, fuel utilization of 0.85, and no cathode off-gas recirculation

Fig. 5 Cathode air flow temperature rise versus current density for various oxygen utilization conditions

with increasing current in the very low current density regime, and decrease for the majority of the operating current range. At very low current densities, the fuel cell is very efficient, but, it provides a smaller fraction of the total system power which lowers system efficiency in this regime.

Note that the heat exchanger effectiveness constraint primarily limits operation in the region of fuel cell current densities greater than about 100 mA/cm^2. The maximum combustor temperature constrains system operation in the high current density, lower fuel utilization regime since a high amount of heat generation in the fuel cell together with high anode off-gas fuel content contributes to higher combustor temperature. The fuel preheater requirements constrain operation in the low current density, high fuel utilization regime, where low heat generation leads to insufficient heat recirculation to preheat the fuel. Thus, the design operating space for the current hybrid SOFC-GT system is constrained to a much smaller region of current density and fuel utilization than that of the entire plot of Fig. 3. Within the allowed design space the maximum system efficiency of nearly 75% is achieved at a current density of 500 mA/cm^2 and fuel utilization of 85%. Depending upon the application of the fuel cell system and the required design flexibility (note this condition is on the margin of not being able to provide sufficient heat for fuel preheat) the desired operating design point of the system may be selected at a different current density or fuel utilization condition. For example, to obtain the more power from the same system (or to lower capital cost) operation at higher current densities may be warranted, but with a concomitant efficiency penalty. For the system considered, it is possible to achieve system efficiencies greater than 70% at 1000 mA/cm^2 and a fuel utilization of 85%.

As shown in Fig. 3, the system design space is bounded by the effects of insufficient energy to properly preheat fuel cell inlet gases at low current densities, maximum achievable hydrogen utilization, mass transfer limitations at high current densities, and combustor temperature limitation at lower hydrogen utilization. The result of these constraints produces a limited region of possible design points where none of these constraints are violated. Note that the presented research focuses on the design space. The operating range of the actual system will be different than the design space. The allowable operating range and performance of specific fuel cell designs have been evaluated by [19,26] and may be considered in subsequent studies for the system designed herein.

Figure 4 displays system efficiency versus current density for variations in oxygen utilization with a constant pressure ratio of 4, fuel utilization of 0.85, and no cathode off-gas recirculation. Applicable system constraints are plotted in the shaded areas. Note that the design space is highly constrained with regard to acceptable oxygen utilization conditions. This is due to the fact that air is both the primary working fluid of the Brayton cycle components
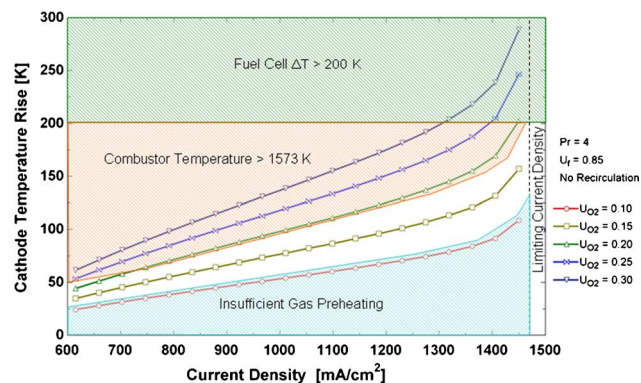
and the primary coolant for the fuel cell component.

At high flow rates (low oxygen utilization), the entirety of the design space is limited because insufficient energy is available to preheat the air and fuel entering the fuel cell. At low air flow rates (high oxygen utilizations); the combustor temperature becomes higher than combustor material limits. The combustor exit temperatures of lower flow rates are very sensitive to oxidation of fuel with insufficient air flow to properly control or limit the combustor temperature. The small design space indicates that the gas turbine flow rate must be well matched to other system components to maintain the fuel cell and combustor operating temperatures with the constraints.

The dependence of system efficiency on oxidant utilization is similar to that of fuel utilization. Note that higher oxygen utilization is always beneficial to system efficiency. But, because of the limited design space, air flow rate manipulation for optimal efficiency is not nearly as important as it is for ensuring safe operating temperatures. At a fuel cell current density of 1000 mA/cm^2 the oxygen utilization should be close to 15%.

Figure 5 shows the effect of current density on the cathode flow temperature rise. The cathode temperature rise only becomes extreme in the regime of very high current density and very low oxygen utilizations. When considering the allowable oxygen utilization and maximum combustor temperature constraint the cathode temperature rise ends up being maintained below 150°C. At a current density of 1000 mA/cm^2, 85% fuel utilization, and the 15% oxygen utilization, the cathode temperature rise is found to be approximately 75°C within the 200°C temperature rise constraint. This indicates that fuel and air preheating constraints and combustor constraints are just as important as fuel cell temperature rise constraints.

4.1.2 Pressure Ratio and System Efficiency. Efficiency tends to increase with increasing pressure ratio for almost all oxygen utilization conditions. However, at some point, increasing pressure ratio decreases system efficiency, which is a behavior somewhat typical of a recuperated Brayton cycle. Figure 6 shows the effect of pressure ratio on system efficiency for various oxygen utilizations at fixed fuel utilization of 0.85, current density of 1000 mA/cm^2, and no cathode off-gas recirculation. Note that the maximum efficiency occurs at lower pressure ratio conditions for the lower oxygen utilization cases. This is due to the fact that lower oxygen utilizations requires larger air flow, which in turn requires more compressor work. The kinks in the curves are associated with the addition of turbine stages. Even though the fuel cell efficiency increases monotonically with pressure, an optimal system pressure is present in these results because of a drop in the recuperated gas turbine efficiency with increasing pressure. Above 5 atms, the increase in fuel cell efficiency with pressure becomes small and the decrease in recuperated gas turbine efficiency results in an overall system efficiency decrease. Note that the ob-
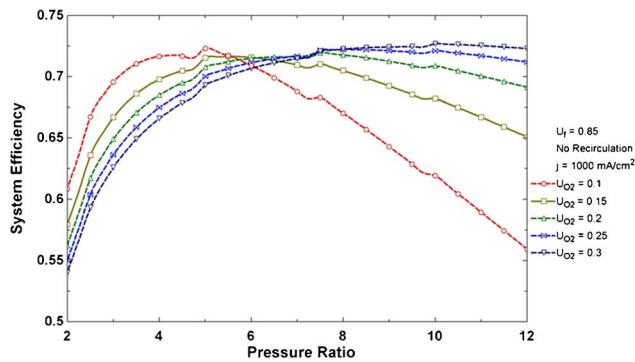
Fig. 6 System efficiency versus pressure ratio for various oxygen utilization conditions

served dependence of system efficiency on pressure ratio is captured because the effects of pressure on turbomachinery isentropic efficiency have been carefully considered.

Note that constraints are not plotted in Fig. 6, but rather, those conditions that are excluded by constraints are plotted as dashed lines. The only results that reside in the acceptable design space are for oxygen utilization of 0.15. At an oxygen utilization of 0.1 the design space is constrained by air and fuel preheat constraints, whereas for utilizations between 0.2 and 0.3 the design space is constrained by combustor temperature limits.

A design pressure ratio of 4 is selected on the basis of results and constraints shown in Fig. 6. A pressure ratio of 4 achieves near maximum efficiency for air flows within design limitations (oxygen utilization near 15%). Furthermore, reduced pressure operation is beneficial in terms of fuel cell seals that become more challenging at higher pressures and lowers the number of compressor and turbine stages (reduces system complexity). So a pressure ratio of 4 is used in all subsequent analyses

4.1.3 Temperature Effects on System Efficiency. When designing the system, it is important to minimize temperature gradients within the fuel cell to lower thermal stresses in the fuel cell. The fuel cell temperature rise relationship with system efficiency was investigated by varying the hydrogen and oxygen utilization and plotting the respective cathode temperature rise versus system efficiency as shown in Fig. 7. The system efficiency and temperature rise both increase with increasing hydrogen utilization. With higher hydrogen utilization the hydrogen flow decreases, resulting in reduced fuel cell anode cooling from the hydrogen flow. Consequently the temperature rise across the fuel cell must increase to remove the heat generated within the fuel cell. However, higher hydrogen utilization results in increased system efficiency result-
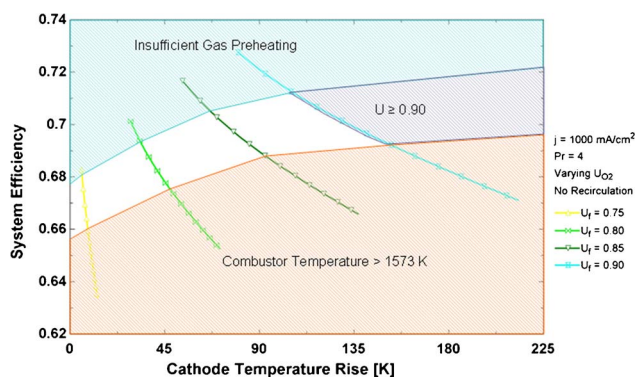

Fig. 7 System efficiency versus cathode air flow temperature rise for various fuel utilization conditions—thermal conductance model

ing in the choice to use air instead of fuel to cool the fuel cell.

It is more practical to cool the fuel cell by manipulating the air flow through the fuel cell as depicted in the results of Fig. 7. A surprising result was found in exploring the system efficiency versus cathode temperature rise. For a given hydrogen utilization the system efficiency is observed to increase with decreasing temperature rise. That is, the system efficiency appears to increase with increasing air flow through the fuel cell. The lowest oxygen utilization was found at the points of highest efficiency for a given hydrogen utilization in Fig. 7.

This result is surprising because previous results show system efficiency decreases with increasing air flow [8,48]. This is certainly true for simple cycle fuel cell systems that have additional blower power losses for increased air flow rates. The case of an SOFC-GT system is more complex, however, since increased air mass flow rates have a counterbalancing increase in turbine power.

The results of Fig. 7 were found to be highly sensitive to the approach that is used to model the heat loss of the system. The heat loss in the current analysis was modeled based on a constant effective thermal conductance and the varying temperature difference, while previous results were obtained by modeling heat loss as proportional to the total fuel energy entering the fuel cell. The current approach accounts for the fact that the fuel cell surface area and insulation will not vary with any particular stack design and arrangement resulting in a relatively constant thermal conductance. Consequently the heat loss in the fuel cell (and combustor) will likely vary with the fuel cell temperature and will remain relatively constant as long as the fuel cell temperature is maintained, even if the air and fuel flow rates vary significantly. Note that in Fig. 7 oxygen utilization was manipulated in the model input tables to vary the air flow through the fuel cell to change the cathode temperature rise (independent variable of Fig. 7).

The result of increasing system efficiency with increased air flow rate (resulting in a decrease in temperature rise in the fuel cell) can be understood by considering an energy balance applied to the entire system. The energy conservation equation of the entire system is

$$\dot{Q}_{\text{fuel}} - \dot{W} = \left(\sum \dot{m}_{\text{out}} h_{\text{out}} - \sum \dot{m}_{\text{in}} h_{\text{in}} \right)$$

or

$$\dot{Q}_{\text{fuel}} = \dot{W} + \left(\sum \dot{m}_{\text{out}} h_{\text{out}} - \sum \dot{m}_{\text{in}} h_{\text{in}} \right) \quad (24)$$

where $\dot{Q}_{\text{fuel}}$ is the total amount of energy added to the system by the heating value of the fuel, $\dot{W}$ is the electrical work output of the system, $\dot{m}$ is the mass flow rate of the working fluid (usually air) at a given point in the system, and h is the enthalpy of the flow corresponding to that state point. In general, $\dot{Q}_{\text{fuel}}$ is fixed for a given power condition, therefore to achieve the maximum system efficiency it is desirable to decrease the proportion of the input energy from the fuel, which leaves the system as exhaust stream enthalpy represented by the magnitude bracketed term in Eq. (24). The value of this term is determined by a tradeoff between how the enthalpy difference between the inlet and outlet streams varies with mass flow rate.

For example, since the inlet enthalpy is generally fixed and determined by ambient conditions, let the inlet temperature be used as the reference temperature, setting the inlet enthalpy to zero. This reduces Eq. (24) to

$$\dot{Q}_{\text{fuel}} = \dot{W} + \left(\sum \dot{m}_{\text{out}} h_{\text{out}} \right) \quad (25)$$

Increasing the mass flow rate would increase the magnitude of the bracketed term. However, depending on system configuration, increasing the mass flow rate may also cause exhaust temperatures to decrease, which would decrease the exhaust enthalpy and contribute to a decrease in the magnitude of the bracketed term. Therefore, the effect that varying the mass flow rate has on the

Table 3 Tradeoff of mass flow rate versus enthalpy change for SOFC-GT hybrid system

Oxygen utilization	$\dot{m}_{exhaust}$ (kg/s)	$h_{exhaust}$ (kJ/kg)	$(\dot{m} \cdot h)_{exhaust}$ (kW)	System efficiency (%)
0.1	255.3	91.96	23,477	71.67
0.15	170.2	149.1	25,376	69.73
0.3	85.1	317.9	27,053	66.59

Fig. 9 System efficiency versus recirculation ratio (ejector) for various oxygen utilization conditions

system efficiency is dependent on which effect is more significant. If the decrease in exhaust enthalpy mathematically outweighs the increase in mass flow rate, then increasing the mass flow rate would increase the system efficiency; if not, then the opposite trend occurs.

In the SOFC-GT system considered here, the final exhaust temperature is allowed to vary. Applying the previous concept to this system, it is evident that increasing the air flow rate increases the system efficiency, since the decrease in exhaust enthalpy outweighs the magnitude of the increase in the air flow rate. The effect of air flow rate on system efficiency is dependent upon system configuration. Due to the complexity and interactions of system components, it is very difficult to evaluate this tradeoff without a detailed analysis of a specific configuration with all component interactions and interdependencies considered, as presented herein. For this particular system configuration, an increase in air flow rate lowers the steady state temperatures of the components in the system with a net benefit on efficiency. A major secondary effect of the temperature decrease is a reduction in heat loss from the SOFC and combustor as simulated by the thermal conductance model, which contributes positively to the increase in efficiency. This secondary effect, when coupled in the modeling and design approach, can be significant in system design evaluation. This is representative of an overall decrease in the bracketed term in Eq. (24) with increasing mass flow rate, and therefore an increased system efficiency, as shown in Table 3.

In different system configurations, such as those with a bottoming steam cycle, the system may be more capable of capturing the exhaust heat, but are constrained by a minimum exhaust temperature due to emissions concerns. In such systems the enthalpy difference between the inlet and exhaust streams would be nearly fixed, and a greater system efficiency would generally be achieved with a decrease in the required air mass flow rate. This effect is also important in describing the behavior of the system with respect to blower recirculation, discussed below.

In addition to the overall mass flow through the fuel cell, the effect of fuel cell operating temperature on the system efficiency is also important. This effect was investigated by varying the cathode temperature rise and cathode outlet temperature directly to
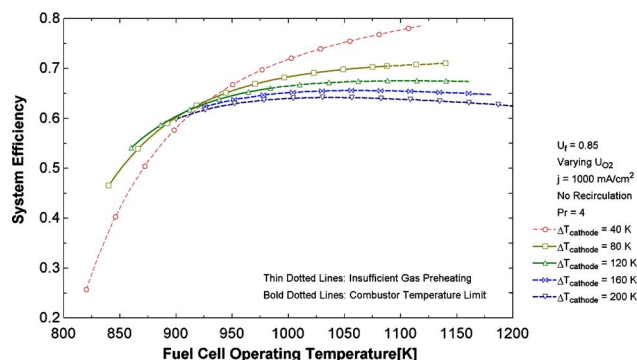

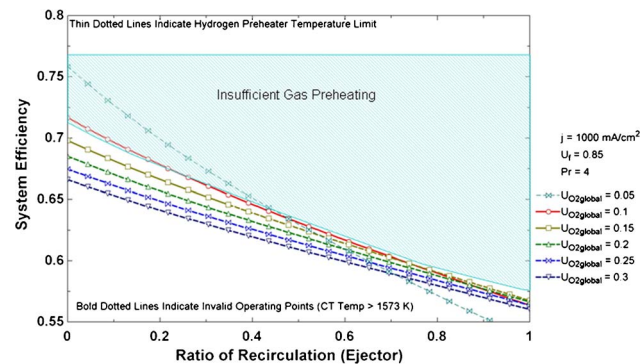**Fig. 8 System efficiency versus fuel cell operating temperature for various cathode temperature difference conditions**

affect the average operating temperature of the fuel cell, as shown in Fig. 8.

The system efficiency tends to increase with an increase in the fuel cell operating temperature, mainly due to the effects of decreased ohmic resistance losses, decreased activation polarizations, and an overall higher turbine inlet temperature for the gas turbine bottoming cycle. This is balanced, however, by a lower Nernst potential at higher average fuel cell operating temperature. Also, since higher fuel cell operating temperatures lead to higher turbine inlet temperatures, the maximum combustor temperature becomes a significant limiting constraint. The results of Fig. 8 demonstrate that the maximum allowable efficiency occurs at the highest possible fuel cell operating temperature that does not lead to conditions that exceed the maximum combustor temperature and maintains sufficient energy to preheat the incoming fuel and air streams by the system exhaust. A moderate temperature rise is preferable, controlled by the effects of the design air flow rate.

4.1.4 Effects of Cathode Exhaust Gas Recirculation. Preheating the flow prior to the fuel cell is of critical importance to SOFC system operation, because the temperature difference across the ceramic cells must be minimized to improve performance (lower temperatures lead to higher polarization) and reduce stress. Air preheating systems are a substantial part of an SOFC system. This part of the study aims to compare different schemes for preheating the cathode inlet air to the required cathode inlet temperature. Cases for cathode exhaust gas recirculation are examined with the use of a blower and an ejector, and each is then compared with the base case that relies on the use of a heat exchanger alone. By recirculating hot cathode off-gas to the inlet, the mass flow through the fuel cell is increased and the inlet temperature is increased.

The primary purpose of using recirculation is to decrease the size of or completely eliminate the need for an air-exhaust heat exchanger (recuperator). Since the fuel cell is the only component of the system that requires a specific flow rate and temperature for operation and cooling, system cost and overall size can be reduced with use of recirculation. This is especially important in aerospace applications, where system weight is a major factor.

4.1.4.1 Ejector recirculation. The effects of air recirculation by means of an ejector on system efficiency and air preheater effectiveness were investigated in detail. Figure 9 displays the effect of increasing ejector recirculation on system efficiency. As the recirculation ratio increases, the system efficiency drops. Similar to the recuperator only case, the global oxygen utilization is limited by the fuel preheater effectiveness or amount of energy available to preheat the fuel cell inlet streams. The dotted curves represent oxygen utilization conditions that are completely limited by the fuel preheater inlet temperature or combustor temperature constraints.

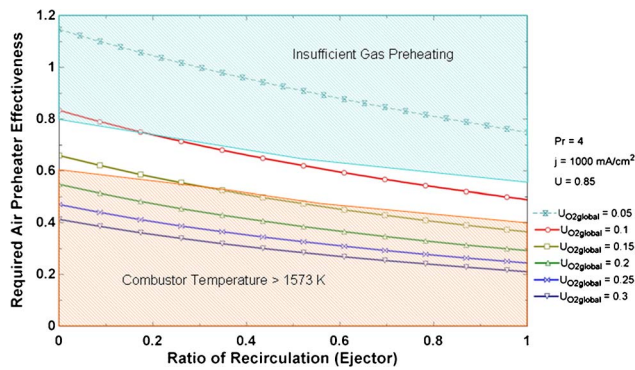The use of an ejector for cathode gas recirculation requires a

Fig. 10 Air preheater effectiveness versus ratio of recirculation (ejector) versus oxygen utilization

Fig. 12 Air preheater effectiveness versus ratio of recirculation (blower) versus oxygen utilization

pressure drop in the ejector that is greater than the respective pressure drop in the recuperator if the flow was solely preheated by means of a recuperator. The pressure drop increases with increasing recirculation ratio, which is the primary cause for the observed decrease in system efficiency with increased recirculation.

Figure 10 displays the effect of ejector recirculation on the effectiveness of the air preheater, and is a measure of how well the ejector recirculation substitutes for using a heat exchanger to preheat the cathode inlet air. A low air preheater effectiveness indicates an ability to downsize the heat exchanger for a given operating point, and indicates that the use of recirculation is a good substitute for the heat exchanger. An air preheater effectiveness of zero on these plots indicates that a heat exchanger is not needed. The air preheater effectiveness decreases monotonically with increasing recirculation ratios. The size of the recuperator can be substantially decreased at the cost of system efficiency within the design space.

Note that the air preheater effectiveness never reaches zero across the current range of recirculation ratios. This indicates that the use of ejector recirculation alone, with a less than unity recirculation ratio, cannot completely substitute for a heat exchanger to fully preheat the cathode inlet air. While some air preheat is inevitable in the "plumbing" that distributes air to the fuel cell stacks, understanding and utilizing this preheat effect is important to the design of SOFC-GT systems that desire to preheat air only using cathode gas recirculation. The range of acceptable oxygen utilization conditions with cathode air recirculation is also limited by combustor temperature and fuel preheating constraints. Note that cathode air recirculation does not significantly expand the allowable design space of the system.
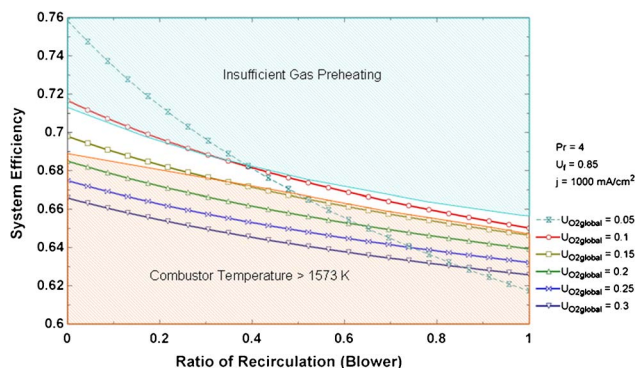

Fig. 11 System efficiency versus recirculation ratio (blower) for various oxygen utilization conditions
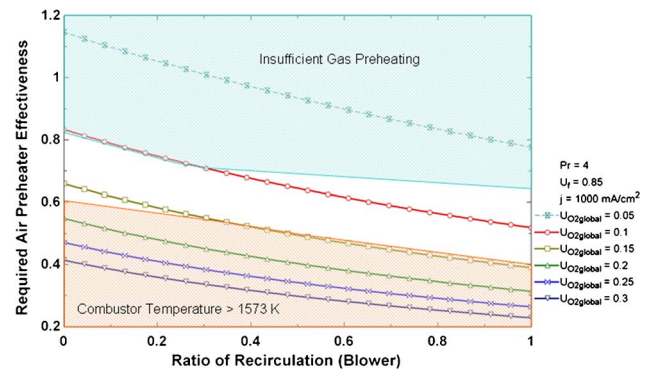
4.1.4.2 Blower recirculation. Instead of using an ejector to recirculate air, it is possible to recirculate cathode air by means of a blower. Figure 11 demonstrates the effect of cathode gas recirculation with the use of a blower on system performance. As the ratio of recirculation increases, the system efficiency decreases with a behavior similar to that of an ejector, but to a smaller extent. Once again, the dotted line represents the lowest oxygen utilization condition, which is completely limited by the fuel preheater inlet temperature constraint.

The main causes of the system efficiency decrease with increasing blower recirculation are increased blower parasitic power requirements, a decrease in the overall mass flow rate, and an increase the system exhaust temperature. The efficiency penalty due to increased exhaust temperature is the most significant. The efficiency penalty due to blower parasitic losses is not as dramatic as that introduced by use of an ejector for the same ratio of recirculation. The impact of heat exchanger pressure losses on system efficiency is smaller than blower parasitic losses, which are in turn smaller than ejector pressure drop losses.

Figure 12 demonstrates the effect of blower recirculation on air preheater effectiveness, used as an indication of how well blower recirculation substitutes for the use of a heat exchanger. Preheating the cathode inlet air with the use of a blower is no more advantageous than an ejector for this specific task. The heat exchanger can simply be downsized with an increasing recirculation ratio.

Recirculation of cathode exhaust gases by use of a blower also shares the same operating limits as that of an ejector or recuperator. As with the ejector, the air recuperator effectiveness never reaches zero for the range considered. It appears that the air recuperator can be substantially decreased in size by using a recirculation blower, but again with a corresponding decrease in system efficiency. A detailed thermo-economical analysis could determine if the capital cost savings associated with reduced recuperator size and gas turbine components outweigh the additional operational cost for lower efficiency operation.

5 Summary and Conclusions

A parametric design study was conducted for a generalized SOFC-GT system. The effects of varying operating parameters, such as current density, pressure ratio, oxygen utilization, and fuel utilization, were studied in the context of an allowable design space. For each parameter studied, a design space was constructed based on constraints of maximum combustor temperature, minimum fuel preheater inlet temperature, maximum air preheater effectiveness, and fuel cell cathode temperature rise. Different schemes of preheating cathode inlet air were studied, such as using a blower or ejector for cathode exhaust gas recirculation, and these cases were compared with the base case of using a heat exchanger only.

The main conclusions of the study are

(1) SOFC-GT system design space is restricted by a maximum combustor temperature at high current densities and low fuel utilization conditions, and the ability to adequately preheat the fuel cell inlet flows at high fuel utilization conditions.

(2) A reasonable design pressure ratio of 4 was found to be a good tradeoff between increased system efficiency and practical simplicity, following the behavior of a typical recuperated axial gas turbine.

(3) The effects of oxygen utilization (which changes the temperature rise through the fuel cell) on system efficiency depend upon system configuration.

(4) Design oxygen utilization is severely limited by the maximum combustor temperature and fuel cell inlet flow preheat constraints.

(5) System efficiency within the design space is restricted by the need to preheat the fuel cell inlet streams, while at the same time providing sufficient flow to cool the fuel cell stacks. For maximum efficiency, maximum amount of heat recuperation is desired (i.e., heat exchanger effectiveness should be as high as possible).

(6) Cathode exhaust gas recirculation can be used to substantially downsize the recuperator in SOFC-GT systems. While using a blower is more efficient than an ejector, cathode air recirculation always results in significant system efficiency reductions.

The parametric analysis indicates the potential design space for SOFC/GT hybrid systems. Overall, the analysis reveals that it is desirable to design hybrid systems with (1) the highest possible fuel utilization, (2) the largest possible air flow, which can be properly preheated prior to the fuel cell, and (3) moderate pressure ratios ($\sim 4-5$) (when using a recuperated axial gas turbine). In hybrid systems, the gas turbine must be carefully integrated and operated to well meet all operating constraints of the fuel cell. Particularly, one must be careful in system design to (1) have sufficient heat to adequately preheat the fuel cell inlet gas streams, (2) maintain combustor temperatures within a tolerable range, and (3) have sufficient air flow to thermally manage the fuel cell. Note that for different system power ranges, the design margins presented herein may change significantly, and this is a topic which should be and must be considered for future studies.

Nomenclature

F = Faraday's constant, C mol^{-1}
$\delta G(T_{fc})$ = Gibbs free energy change as a function of fuel cell temperature, kJ kg^{-1}
h = enthalpy of flow, kJ kg^{-1}
i = Current, A
j = current density, mA cm^{-2}
k = specific heat ratio
$\dot{m}$ = mass flow rate, kg s^{-1}
n = number of participating electrons in electrochemical reaction
$n$cells = number of cells
$n$stacks = number of fuel cell stacks–
$\dot{N}$ = molar flow rate, K mol s^{-1}
N_s = number of turbine stages
P = pressure, kPa
$\dot{Q}$ = rate of heat transfer, kW
$\dot{\tilde{R}}$ = molar reaction rate K mol s^{-1}
R = universal gas constant J mol^{-1} K^{-1}
R_{eff} = effective area specific resistance ohm
T = temperature, K
U_f = fuel utilization

U_{O_2} = oxygen utilization
U_{ht} = overall thermal conductance coefficient kW K^{-1}
V = Voltage, V
$\dot{w}$ = power output or requirement, kW
w = ratio of recirculation
X = mole fraction
η = isentropic efficiency of component
η_{cp} = polytropic efficiency of compressor

References

[1] Williams, M. C., Strakey, J., and Sudoval, W., 2006, "U.S. DOE Fossil Energy Fuel Cells Program," J. Power Sources, **159**(2), pp. 1241–1247.

[2] Verma, A., Rao, A. D., and Samuelsen, G. S., 2006, "Sensitivity Analysis of a Vision 21 Coal Based Zero Emission Power Plant," J. Power Sources, **158**(1), pp. 417–427.

[3] Daggett, D., Eelman, S., and Kristiansson, G., 2003, "Fuel Cell APU," AIAA International Air and Space Symposium and Exposition: The Next 100 Years, July 14–17, Dayton, OH.

[4] Kohout, L. L., and Schmitz, P. C., 2003, "Fuel Cell Propulsion Systems for an All-Electric Personal Air Vehicle," NASA Report No. TM-2003-212354.

[5] Colozza, A. J., 2002, Hydrogen Storage for Aircraft Applications Overview, NASA Report No. CR-2002-211867.

[6] Heinzel, A., Hebling, C., Muller, M., Zedda, M., and Muller, C., 2002, "U.S. DOE Fossil Energy Fuel Cells Program," J. Power Sources, **105**(2), pp. 250–255.

[7] Koroneos, C., and Dompros, A., 2005, "Advantages of the Use of Hydrogen Fuel as Compared to Kerosene," Resour. Conserv. Recycl., **44**(2), pp. 99–113.

[8] Zhang, X., Li, J., Li, G., and Feng, Z., 2007, "Cycle Analysis of an Integrated Solid Oxide Fuel Cell and Recuperative Gas Turbine With an Air Reheating System," J. Power Sources, **164**(2), pp. 752–760.

[9] Rao, A. D., and Samuelsen, G. S., 2003, "A Thermodynamic Analysis of Tubular Solid Oxide Fuel Cell Based Hybrid Systems," ASME J. Eng. Gas Turbines Power, **125**(1), pp. 59–66.

[10] Calise, F., Dentice d'Accadia, M., Palombo, A., and Vanoli, L., 2006, "Simulation and Exergy Analysis of a Hybrid Solid Oxide Fuel Cell (SOFC)-Gas Turbine System," Energy, **31**(15), pp. 3278–3299.

[11] Calise, F., Palombo, A., and Vanoli, L., 2006, "Design and Partial Load Exergy Analysis of Hybrid SOFC-GT Power Plant," J. Power Sources, **158**(1), pp. 225–244.

[12] Chan, S. H., Low, C. F., and Ding, O. L., 2002, "Energy and Exergy Analysis of Simple Solid-Oxide Fuel-Cell Power Systems," J. Power Sources, **103**(2), pp. 188–200.

[13] Yang, W. J., Park, S. K., Kim, T. S., Kim, J. H., Sohn, J. L., and Ro, S. T., 2006, "Design Performance Analysis of Pressurized Solid Oxide Fuel Cell/Gas Turbine Hybrid Systems Considering Temperature Constraints," J. Power Sources, **160**(1), pp. 462–473.

[14] Zhang, X., Li, J., Li, G., and Feng, Z., 2006, "Dynamic Modeling of a Hybrid System of the Solid Oxide Fuel Cell and Recuperative Gas Turbine," J. Power Sources, **163**(1), pp. 523–531.

[15] Kuchonthara, P., Bhattacharya, S., and Tsutsumi, A., 2003, "Energy Recuperation in Solid Oxide Fuel Cell (SOFC) and Gas Turbine (GT) Combined System," J. Power Sources, **117**(1–2), pp. 7–13.

[16] Chan, S. H., Ho, H. K., and Tian, Y., 2002, "Modelling of Simple Hybrid Solid Oxide Fuel Cell and Gas Turbine Power Plant," J. Power Sources, **109**(1), pp. 111–120.

[17] Park, S. K., Oh, K. S., and Kim, T. S., 2007, "Analysis of the Design of a Pressurized SOFC Hybrid System Using a Fixed Gas Turbine Design," J. Power Sources, **170**(1), pp. 130–139.

[18] Costamagna, P., Magistri, L., and Massardo, A. F., 2001, "Design and Part-Load Performance of a Hybrid System Based on a Solid Oxide Fuel Cell Reactor and a Micro Gas Turbine," J. Power Sources, **96**(2), pp. 352–368.

[19] Calise, F., Dentice d'Accadia, M., Vanoli, L., and von Spakovsky, M. R., 2007, "Full Load Synthesis/Design Optimization of a Hybrid SOFC-GT Power Plant," Energy, **32**(4), pp. 446–458.

[20] Calise, F., Dentice di Accadia, M., Vanoli, L., and von Spakovsky, M. R., 2006, "Single-Level Optimization of a Hybrid SOFC-GT Power Plant," J. Power Sources, **159**(2), pp. 1169–1185.

[21] Park, S. K., and Kim, T. S., 2006, "Comparison Between Pressurized Design and Ambient Pressure Design of Hybrid Solid Oxide Fuel Cell-Gas Turbine Systems," J. Power Sources, **163**(1), pp. 490–499.

[22] Aguiar, P., Adjiman, C. S., and Brandon, N. P., 2005, "Anode-Supported Intermediate-Temperature Direct Internal Reforming Solid Oxide Fuel Cell: II. Model-Based Dynamic Performance and Control," J. Power Sources, **147**(1–2), pp. 136–147.

[23] Xue, X., Tang, J., Sammes, N., and Du, Y., 2005, "Dynamic Modeling of Single Tubular SOFC Combining Heat/Mass Transfer and Electrochemical Reaction Effects," J. Power Sources, **142**(1–2), pp. 211–222.

[24] Stiller, C., Thorud, B., Bolland, O., Kandepu, R., and Imsland, L., 2006, "Control Strategy for a Solid Oxide Fuel Cell and Gas Turbine Hybrid System," J. Power Sources, **158**(1), pp. 303–315.

[25] Mueller, F., Brouwer, J., Jabbari, F., and Samuelsen, S., 2006, "Dynamic Simulation of an Integrated Solid Oxide Fuel Cell System Including Current-

Based Fuel Flow Control," ASME J. Fuel Cell Sci. Technol., **3**(2), pp. 144–154.

[26] Milewski, J., Miller, A., and Salacinski, J., 2007, "Off-Design Analysis of SOFC Hybrid System," Int. J. Hydrogen Energy, **32**(6), pp. 687–698.

[27] Yi, Y., Rao, A. D., Brouwer, J., and Samuelsen, G. S., 2004, "Analysis and Optimization of a Solid Oxide Fuel Cell and Intercooled Gas Turbine (SOFC-ICGT) Hybrid Cycle," J. Power Sources, **132**(1–2), pp. 77–85.

[28] Winkler, W., and Lorenz, H., 2002, "The Design of Stationary and Mobile Solid Oxide Fuel Cell-Gas Turbine Systems," J. Power Sources, **105**(2), pp. 222–227.

[29] Chan, S. H., Ho, H. K., and Tian, Y., 2003, "Multi-Level Modeling of SOFC-Gas Turbine Hybrid System," Int. J. Hydrogen Energy, **28**(8), pp. 889–900.

[30] FChart-Software, 2008, EES Manual.

[31] F-Chart Software, 2008, Engineering Equation Solver (EES), Madison, WI.

[32] Burt, A. C., Celik, I. B., Gemmen, R. S., and Smirnov, A. V., 2004, "A Numerical Study of Cell-to-Cell Variations in a SOFC Stack," J. Power Sources, **126**(1–2), pp. 76–87.

[33] Campanari, S., and Iora, P., 2004, "Definition and Sensitivity Analysis of a Finite Volume SOFC Model for a Tubular Cell Geometry," J. Power Sources, **132**(1–2), pp. 113–126.

[34] Yoon, K. J., Zink, P., Gopalan, S., and Pal, U. B., 2007, "Polarization Measurements on Single-Step Co-Fired Solid Oxide Fuel Cells (SOFCs)," J. Power Sources, **172**(1), pp. 39–49.

[35] Balan, C., Dey, D., Eker, S.-A., Peter, M., Sokolov, P., and Wotzak, G., 2004, "Coal Integrated Gasification Fuel Cell System Study Final Report," Hybrid Power Generation Systems, Torrance, CA. Report No. DE-FC26-01NT40779.

[36] Baskharone, E. A., 2006, *Principles of Turbomachinery in Air Breathing Engines*, Cambridge University Press, New York.

[37] Kim, S., and Kwon, S., 2006, "Experimental Determination of Geometric Parameters for an Annular Injection Type Supersonic Ejector," ASME J. Fluids Eng., **128**, pp. 1164–1171.

[38] Zhu, Y., Cai, W., Wen, C., and Li, Y., 2007, "Fuel Ejector Design and Simulation Model for Anodic Recirculation SOFC System," J. Power Sources, **173**(1), pp. 437–449.

[39] Ferrari, M. L., Bernardi, D., and Massardo, A. F., 2006, "Design and Testing of Ejectors for High Temperature Fuel Cell Hybrid Systems," ASME J. Fuel Cell Sci. Technol., **3**, pp. 284–291.

[40] Marsano, F., Magistri, L., and Massardo, A. F., 2004, "Ejector Performance Influence on a Solid Oxide Fuel Cell Anodic Recirculation System," J. Power Sources, **129**(2), pp. 216–228.

[41] Freeh, J. E., Pratt, J. W., and Brouwer, J., 2004, "Development of a Solid-Oxide Fuel/Cell Gas Turbine Hybrid System for Aerospace Applications," NASA Glenn Research Center Report No. TM-2004-213054.

[42] Kim, J.-W., Virkar, A. V., Fung, K.-Z., Mehta, K., and Singhal, S. C., 1999, "Polarization Effects in Intermediate Temperature, Anode-Supported Solid Oxide Fuel Cells," J. Electrochem. Soc., **146**(1), pp. 69–78.

[43] Mueller, F., Gaynor, R., Auld, A. E., Brouwer, J., Jabbari, F., and Samuelsen, G. S., "Synergistic Integration of a Gas Turbine and Solid Oxide Fuel Cell for Improved Transient Capability," J. Power Sources, in press.

[44] Mueller, F., Jabbari, F., Brouwer, J., Roberts, R., Junker, T., and Ghezel-Ayagh, H., 2007, "Control Design for A Bottoming Solid Oxide Fuel Cell Gas Turbine Hybrid System," ASME J. Fuel Cell Sci. Technol., **4**, pp. 221–230.

[45] Kandepu, R., Imsland, L., Foss, B. A., Stiller, C., Thorud, B., and Bolland, O., 2007, "Modeling and Control of a SOFC-GT-Based Autonomous Power System," Energy, **32**(4), pp. 406–417.

[46] Santarelli, M., Leone, P., Cali, M., and Orsello, G., 2007, "Experimental Evaluation of the Sensitivity to Fuel Utilization and Air Management on a 100 kW SOFC System," J. Power Sources, **171**(1), pp. 155–168.

[47] Nehter, P., 2007, "A High Fuel Utilizing Solid Oxide Fuel Cell Cycle With Regard to the Formation of Nickel Oxide and Power Density," J. Power Sources, **164**(1), pp. 252–259.

[48] Stiller, C., Thorud, B., Seljebø, S., Mathisen, Ø., Karoliussen, H., and Bolland, O., 2005, "Finite-Volume Modeling and Hybrid-Cycle Performance of Planar and Tubular Solid Oxide Fuel Cells," J. Power Sources, **141**(2), pp. 227–240.